

## Research Article



## Subduction earthquake cycles controlled by episodic fluid pressure cycling

Luca Dal Zilio <sup>a,\*</sup>, Taras Gerya <sup>b</sup><sup>a</sup> Seismology and Geodynamics, Institute of Geophysics, Department of Earth Sciences, Swiss Federal Institute of Technology (ETH Zürich), Zürich, Switzerland<sup>b</sup> Geophysical Fluid Dynamics, Institute of Geophysics, Department of Earth Sciences, Swiss Federal Institute of Technology (ETH Zürich), Zürich, Switzerland

## ARTICLE INFO

## Keywords:

Rock-fluid interaction  
Earthquake cycles  
Subduction megathrust  
Fault mechanics  
Hydraulic properties

## ABSTRACT

In subduction zones, fluids are often invoked to explain slip processes on the megathrust, from great earthquakes to slow-slip events and tectonic tremors. However, it is unclear how the transient evolution of pore-fluid is controlled by depth-dependent variations in hydraulic properties over a broad range of timescales concomitant with the full spectrum of seismic and aseismic slip. In this study, we leverage a newly-developed fully dynamic hydro-mechanical earthquake cycle modeling framework to simulate fluid-driven seismic and aseismic fault slip. By assimilating geological, geophysical, and laboratory data in a physics-based model of fault dynamics, we investigate the role of hydraulic properties on-fault in controlling the predominant slip mode along the subduction megathrust. Results indicate that fluid-driven shear cracks nucleate due to a competing mechanism between the compaction of pores and the dynamic self-pressurization of fluids inside the megathrust, whereas the subsequent propagation of dynamic ruptures is self-sustained by solitary pore-pressure waves. While models with uniform hydraulic properties yield to regular seismic cycles of complete megathrust ruptures, a depth-varying fault permeability leads to the emergence of complex aperiodic sequences characterized by partial and complete ruptures, aftershocks, and transient aseismic slip. Further parameter analysis shows that the slip response on-fault primarily depends on fault permeability and porosity, which in turn control the poroelastic compaction, the storage capacity, and the hydraulic diffusion length. Four slip response patterns are revealed by the parameter space, including seismic events, slow-slip events, oscillatory decay with time, and stable aseismic creep. Our findings provide new insights into the interplay between pore-fluid, mechanical, and fault slip processes, and suggest that solid-fluid interactions and the permeability architecture play a key role in controlling the predominant slip mode on subduction megathrusts.

## 1. Introduction

Fluids, tectonic deformation, and earthquake source processes are intrinsically linked. Over the last decades, there has been a general recognition that fluids are not a passive elements of tectonic environments, but rather an integral component of tectonic, faulting, and earthquake processes (e.g., Miller, 2013; Saffer and Tobin, 2011). The most abundant fluid affecting tectonic and seismic processes in subduction zones is water ( $H_2O$ ), which is present either in hydrous minerals or as fluid phase percolating through porous rocks in response to plate bending-related fracturing and faulting at the trench-rise system (Faccenda, 2014; Kerrick and Connolly, 1998; Peacock, 1990; Schmidt and Poli, 1998) (Fig. 1a). Abundant  $H_2O$  released by dehydration reactions cause an increase in pore pressure, particularly when fluids are capped by low permeability barriers (Audet et al., 2009; Gao and Wang, 2017). Occasional breaching of these barriers is commonly described by

the fault-valving model (Sibson, 1990). Evidence of elevated pore-fluid pressures comes from earthquake focal mechanisms and tomographic imaging of elastic properties around the source region of slow-slip phenomena (Audet et al., 2009; Audet et al., 2010; Matsubara et al., 2009; Shelly et al., 2006; Song et al., 2009; Warren-Smith et al., 2019). These studies show that tectonic tremor and slow-slip events occur preferentially in regions with high ratios of compressional- to shear-wave seismic velocity ( $V_p/V_s$ ), or ultralow shear-velocity layers (Peng and Gomberg, 2010).

How does water influence seismic and aseismic slip on subduction megathrusts? There is no clear answer to this question, but competing effects are expected on theoretical grounds: elastic dislocation theory combined with constitutive laws of rock friction (Dieterich, 2007; Marone, 1998) suggest that pore-fluid pressure may inhibit dynamic instabilities that lead to earthquake nucleation. High pore-fluid pressure causes a reduction in the effective normal stress, which promotes stable

\* Corresponding author.

E-mail address: [luca.dalzilio@erdw.ethz.ch](mailto:luca.dalzilio@erdw.ethz.ch) (L. Dal Zilio).

aseismic slip, rather than dynamic earthquake rupture (Ikari et al., 2013; Scholz, 1998; Segall and Rice, 1995). While poroelastic effects can destabilize rate-strengthening faults (Heimisson et al., 2019), dilatancy during fault slip could counteract pore pressurization and promote stability (Dal Zilio et al., 2020a; Liu and Rubin, 2010; Segall and Rice, 1995), whereas pore pressurization due to shear heating should promote fault failure (Noda and Lapusta, 2013; Rice, 2006; Sibson, 1973). The critical nucleation size (the minimum size that an aseismically creeping patch must reach for slip to become unstable) is inversely proportional to the effective normal stress (Rice and Ruina, 1983; Rubin and Ampuero, 2005), so that a pore-pressure increase should promote failure but inhibit the onset of seismic slip. It is thus unclear whether a pore-pressure increase due to natural sealing and compaction of a fault zone should promote seismic or aseismic slip. This controversy poses a major challenge in our understanding of earthquake physics, with severe implications for seismic hazard. This problem is particularly challenging because the transient evolution of pore-fluid in active faults is controlled by depth-dependent variations in hydraulic properties over a broad range of timescales (Saffer and Tobin, 2011; Sun et al., 2020).

In this study, we leverage a newly-developed hydro-mechanical earthquake cycles modeling framework to evaluate how water controls the slip behavior on megathrust faults. Fully dynamic simulations of earthquake sequences in a poro-visco-elasto-plastic compressible medium provide a bridge between a broad range of spatiotemporal scales harnessing the ability to model solid-fluid interaction processes and to uncover the physical mechanisms and parameters relevant to naturally complex megathrust faults. We provide a set of numerical experiments in which we change the initial hydraulic conditions to evaluate megathrust slip characteristics over multiple earthquake cycles. We show that the evolution of pore-fluid pressure and the associated reduction of strength on-fault control the slip mode and, in turn, the spatial distribution of earthquakes. Furthermore, the model reveals that a depth-dependent permeability is a dominant factor in controlling complex aperiodic sequences characterized by partial and complete ruptures, as well as aftershocks and transient aseismic slip. To this end, we explore the parameter space to determine how fault permeability and porosity control the predominant slip mode. These results demonstrate that on-fault hydraulic properties either inhibit or facilitate fault slip and rupture propagation and uncover the underlying physics that allows earthquakes and slow-slip events to occur on the same fault segment.

## 2. Methods

### 2.1. Hydro-mechanical earthquake cycles

The employed numerical code H-MEC (Dal Zilio et al., 2022a) combines conservative finite differences in a fully staggered grid and marker-in-cell techniques. The total momentum (solid matrix and fluid phase), fluid momentum, compressible solid mass, and compressible fluid mass are implicitly solved using a poro-visco-elasto-plastic rheology on the non-deforming Eulerian grid. Physical properties including strain rate, viscosity, porosity and permeability are transported through the motion of Lagrangian particles, which are advected by the velocity field interpolated from the Eulerian grid (Gerya and Yuen, 2007). The total momentum equations account for inertial wave-mediated dynamics to stabilize high slip rates at small time steps.

The governing equations contain poroelasticity terms consistent with Biot's theory (Biot, 1941; Gassmann, 1951; Petrini et al., 2020; Yarushina and Podladchikov, 2015), including the Biot-Willis coefficient (Biot and Willis, 1957) and the Skempton coefficient (Bishop, 1973; Skempton, 1960), which allow for a fully coupled pressure-based compressible formulation. This hydro-mechanical system thus accounts for the compressibility of both solid matrix and fluid phase through the elastic (reversible) and visco-plastic (irreversible) compaction/decompaction of the interconnected porous space. Furthermore, it is worth noting that our numerical simulations incorporate inertial wave-mediated effects, thus making the model fully dynamic. Without additional weakening mechanisms, quasi-dynamic models (adopting a radiation damping term) and fully dynamic models generate qualitatively similar slip patterns with quantitative differences. For example, quasi-dynamic models typically produce smaller stress drops, slower slip velocities, and slower rupture speeds during earthquakes and more propensity for ruptures to arrest at the velocity-strengthening patch (Thomas et al., 2014). However, fully dynamic simulations with additional coseismic weakening produce qualitatively different patterns of earthquakes, with near-periodic pulse-like events. Full details of this method, including the description of the continuum-based model and the discretization of governing equations, are provided in Dal Zilio et al. (2022a).

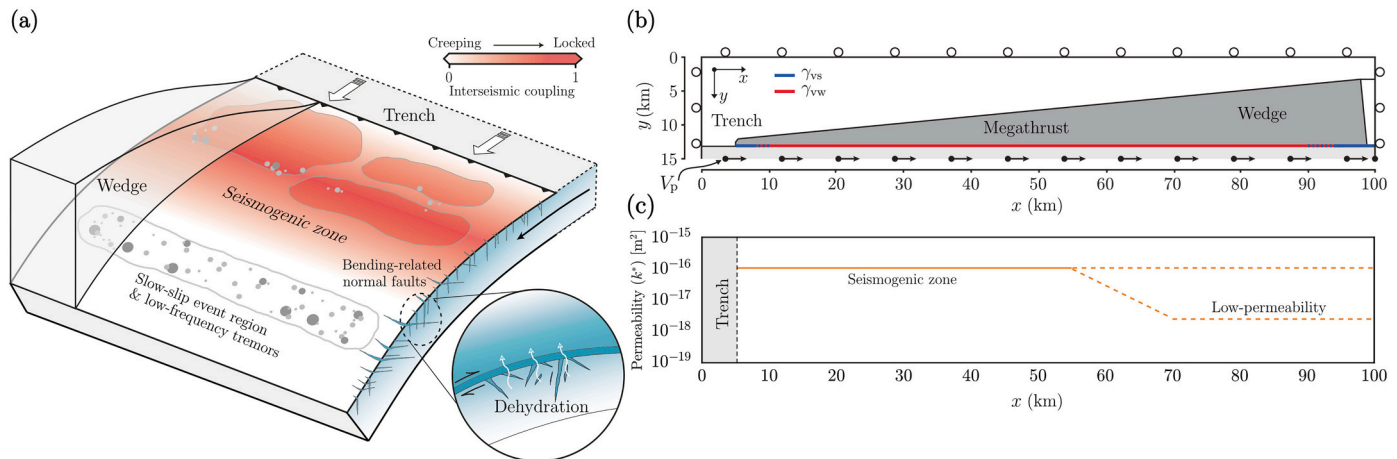


**Fig. 1.** Conceptual model and initial setup. (a) Sketch of a generic subduction megathrust displaying the seismogenic zone with the typical distribution of inter-seismic coupling and a deeper slow-slip event region. The zoomed sketch highlights the bending-related normal faults and the percolation of fluids from the subducting slab to the plate interface. (b) Model setup of a simplified subduction zone adopted from Dal Zilio et al. (2022b) with a planar megathrust embedded in a homogeneous poro-visco-elasto-plastic medium. Boundary conditions include: free slip (small rollers) at the top, left, and right boundaries, whereas tangential displacement (small arrows) is prescribed at the bottom boundary. (c) Downdip permeability distribution on the megathrust, which assumes either a constant permeability or a depth-dependent permeability.

## 2.2. Poro-visco-elasto-plastic rheology

The employed poro-visco-elasto-plastic rheology is based on a constitutive relationship between deviatoric strain rate ( $\dot{\epsilon}'_{ij}$ ) and stresses ( $\tau_{ij}$ ), and decomposed into its elastic, viscous, and plastic components as

$$\dot{\epsilon}'_{ij} = \left[ \dot{\epsilon}'_{ij} \right]_{\text{viscous}} + \left[ \dot{\epsilon}'_{ij} \right]_{\text{elastic}} + \left[ \dot{\epsilon}'_{ij} \right]_{\text{plastic}}$$

$$= \frac{\tau_{ij}}{2\eta_s} + \frac{1}{2\mu} \frac{\tilde{D}}{Dt} (\tau_{ij}) + \begin{cases} 0 & \rightarrow \tau_{II} < \tau_y \\ \chi \frac{\partial Q}{\partial \tau_{ij}} = \chi \frac{\tau_{ij}}{\tau_{II}} & \rightarrow \tau_{II} = \tau_y \end{cases} \quad (1)$$

where  $\eta_s$  is the effective shear viscosity,  $\tilde{D}/Dt$  is the objective co-rotational time derivative,  $\mu$  is the shear modulus,  $\chi$  is the *plastic multiplier* to ensure that, when yielding occurs, the square root of the second invariant of the deviatoric stress tensor ( $\tau_{II} = \sqrt{\tau_{xx}^2 + \tau_{xy}^2}$ ) always satisfies the yield stress  $\tau_y$ . The non-associated plastic flow law is defined through the *plastic flow potential* ( $Q$ ), which reflects the amount of mechanical energy per unit volume that supports plastic deformation (Vermeer, 1998)

$$Q = \tau_{II} - \sin(\psi) (p^{[t]} - p^{[f]}) - \cos(\psi) c. \quad (2)$$

In this study we assume a plastic flow potential with zero dilation angle ( $\psi = 0$ ).

Plastic deformation and frictional slip is treated in the framework of continuum plasticity and accurately solved via Picard iterations (Dal Zilio et al., 2022a). In particular, the method is based on a Drucker-Prager-type yield criterion (Prager and Drucker, 1952) combined with a rate dependent plasticity model (Yi et al., 2018)

$$\tau_y = \tau_0 \left( \frac{\dot{\epsilon}_{II[p]}}{\varepsilon_0} \right)^\gamma, \quad (3)$$

$$\tau_0 = c + f (p^{[t]} - p^{[f]}) \quad (4)$$

where  $\varepsilon_0$  is the reference strain rate,  $c$  is the cohesion,  $f$  is the static friction coefficient,  $p^{[t]}$  and  $p^{[f]}$  are the total and fluid pressure, respectively, and  $\dot{\epsilon}_{II[p]}$  is the second invariant of the deviatoric plastic strain rate

$$\dot{\epsilon}'_{II[p]} = \varepsilon_0 \left( \frac{\tau_{II}}{\tau_0} \right)^{1/\gamma}, \quad (5)$$

where  $\gamma$  is the rate-strengthening exponent controlling the “direct effect”, i.e., the transient increase of the shear strength due to instantaneous changes in slip velocity, a feature that has ample laboratory confirmation (Dieterich, 1979, 1981; Marone, 1998; Ruina, 1983). In this work,  $\gamma = 0.010$  is used in the seismogenic zone, while both the up-dip and down-dip limits of megathrust assume  $\gamma = 0.100$  (see Fig. 1b and Table 1). The slip rate ( $V$ ) is quantified as the second invariant of deviatoric plastic strain rate  $\dot{\epsilon}_{II(p)}$  integrated across the fault zone width  $w_h$

$$V = 2 \dot{\epsilon}'_{II[p]} w_h. \quad (6)$$

Plastic deformation is computed as volumetric strain and is represented by a tensor. Consequently, plastic yielding can spontaneously localize anywhere (Dal Zilio et al., 2022a, 2022b).

The deviatoric stress is computed from the visco-elasto-plastic constitutive relationships (Eq. (1)) by using an implicit first-order finite-difference scheme in time in order to represent objective time derivatives of visco-elastic stresses (e.g., Gerya, 2019; Moresi et al., 2003)

**Table 1**  
Model parameters.

Parameter	Symbol	Value
x-domain	$L_x$	100 km
y-domain	$L_y$	20 km
Grid resolution	$\Delta_x$	100 m
Shear modulus	$\mu$	25 GPa
Bulk modulus	$K$	50 GPa
Rate-strengthening parameter:		
Seismogenic zone	$\gamma_{vw}$	0.010
Up- & down-dip	$\gamma_{vs}$	0.100
Poisson ratio	$\nu$	0.25
Total pressure	$p^{[t]}$	50 MPa
Fluid pressure	$p^{[f]}$	10 MPa
Solid density	$\rho^{[s]}$	2900 kg m <sup>-3</sup>
Fluid density	$\rho^{[f]}$	1000 kg m <sup>-3</sup>
Solid compressibility	$\beta^{[s]}$	2.5 10 <sup>-11</sup> 1/Pa
Fluid compressibility	$\beta^{[f]}$	4.0 10 <sup>-10</sup> 1/Pa
Solid viscosity	$\eta_0$	10 <sup>21</sup> Pa s
Fluid viscosity	$\eta^{[f]}$	10 <sup>-3</sup> Pa s
Shear wave speed	$c_s$	$\sqrt{\mu/\rho^{[f]}}$
Gravity	$g$	9.81998 m s <sup>-2</sup>
Reference friction	$f$	0.6
Cohesion	$c$	3.0 MPa
Fault width	$h$	100 m
Critical nucleation size	$L_c$	6.7 km
Cohesive zone size	$\Lambda_0$	2.1 km
Reference velocity	$V_0$	10 <sup>-9</sup> m s <sup>-1</sup>
Reference strain rate	$\varepsilon_0$	$V_0/(2\Delta_x)$
Reference porosity	$\phi^*$	1%
Reference permeability	$k^*$	10 <sup>-16</sup> m <sup>2</sup>
Loading velocity (plate rate)	$V_p$	2.5 · 10 <sup>-9</sup> m s <sup>-1</sup>

$$\tau_{ij} = 2\eta_{vp} Z \dot{\epsilon}'_{ij} + \tau_{ij}^0 (1 - Z), \quad (7)$$

where  $Z$  is the visco-elasticity factor (Schmalholz et al., 2001)

$$Z = \frac{\mu \Delta t}{\mu \Delta t + \eta_{vp}}. \quad (8)$$

$\Delta t$  is the computational time step and  $\eta_{vp}$  is the effective visco-plastic viscosity that characterizes the intensity of the visco-plastic deformation:

$$\eta_{vp} = \begin{cases} \eta_m & \rightarrow \tau_{II} < \tau_y \\ \eta_m \frac{\tau_{II}}{2\eta_m \dot{\epsilon}_{II[p]} + \tau_{II}} & \rightarrow \tau_{II} = \tau_y \end{cases}, \quad (9)$$

where  $\eta_m$  is the *matrix viscosity* (Katz et al., 2006)

$$\eta_m = \eta_s e^{(\lambda - \phi)} \quad (10)$$

in which  $\lambda = -29$  defines an experimentally derived porosity-weakening coefficient (Katz et al., 2006). It should be noted that our simplified hydro-mechanical subduction model neglects porosity evolution with time. In nature, porosity evolution of subduction interface rocks would be affected by the competition between visco-elasto-plastic compaction considered in our mass conservation equations and temperature-dependent rock dehydration processes (Gerya and Meilick, 2011; Poulet et al., 2014), which is not taken into account. It should also be noted that seismic cycle time scales considered here are relatively short compared to porosity evolution timescales (Petrini et al., 2020). A detailed description of the rheological constitutive equations is given in Dal Zilio et al. (2022a).

## 2.3. Model setup

The 2-D model setup consists in a computational domain of 100 × 20 km in x- and y-directions, respectively (Fig. 1). The Eulerian grid consists of 1000 × 200 nodal points, which result in a spatial resolution

of 100 m. Each cell contains 16 Lagrangian particles carrying material properties of their rock phase. An adapting free-surface boundary condition is employed along the wedge surface (Dal Zilio et al., 2022b), which allows the free-surface viscosity to decrease by several orders of magnitudes during the propagation of dynamic rupture, i.e., when the computational time step is of the order of milliseconds and the maximum slip rate on the fault is of the order of meters per second. Except for the left and right side of the model, the velocity boundary conditions resemble those of an analog sandbox model (Dal Zilio et al., 2020b): The top, left, and right boundaries have a free-slip boundary condition (zero shear stress), whereas the lower boundary has an imposed loading rate of 4 cm/yr.

Several studies suggest that the megathrust permeability decreases with depth for a number of reasons: (1) volumetric expansion due to serpentinization (Wada et al., 2008), which reduces grain boundary connectivity and, in turn, permeability; (2) large deposits of silica ( $\text{SiO}_2$ ) from slab-derived fluids (Audet and Bürgmann, 2014); and (3) stacking of relict shear zones atop the active plate boundary (Delph et al., 2021). To account for such variability, in this study we test constant hydraulic properties and a depth-varying permeability on the fault zone (Fig. 1c). The initial geometry portrays a simplified subduction zone and consists of a megathrust between a planar subducting slab and an overlying wedge. While the megathrust has a fixed dip angle, the 2-D plane strain model is designed such that physical properties vary in the downdip direction. The visco-elasto-plastic parameters are listed in Table 1.

### 3. Results

In this section, we present models that assume both homogeneous hydraulic properties and a depth-dependent distribution of permeability (Fig. 1c). We then investigate the parameter space between the fault porosity and the fault permeability. This large dataset allows us to assess the fault behavior over several earthquake cycles, the predominant slip mode, and the role of fault porosity and permeability in controlling the seismic and aseismic slip pattern on the megathrust.

#### 3.1. Homogeneous hydraulic properties

The megathrust response to tectonic loading is characterized by periods of interseismic quiescence of quasi-static deformation followed by rapid slip events (Fig. 2). Given the constant and homogeneous hydraulic properties on the fault, the long-term fault behavior shows similar features of earthquake recurrence and interseismic periods, with fault slip rates varying between  $\sim 10^{-9}$  and  $\sim 1 \text{ m s}^{-1}$  (Fig. 2a). Due to the rate-strengthening rheology (Eq. (3)), the interseismic periods are characterized by stable aseismic creep in which the shear stress increases over time and interseismic slip propagates from the lower limit of the fault towards the downdip edge of the seismogenic zone (Fig. 2b). Earthquakes spontaneously nucleate near the downdip edge of the seismogenic zone, and the resulting dynamic ruptures propagate across the seismogenic fault mostly unilaterally towards the trench. Following the complete rupture and related stress drop, the megathrust hosts postseismic slip through the entire ruptured fault segment, particularly in the rate-strengthening updip and downdip limits of the seismogenic zone.

Our modeling indicates that an increase in the slip velocity due to a seismic event is associated with an abrupt increase of pore-fluid pressure within the fault zone, which can dynamically increase by several MPa (Fig. 3). The increase in pore-fluid pressure is simultaneously coupled to a rapid decrease in viscosity and localized strain rate (Fig. 3a). Notably, at coseismic slip rates, the effective shear viscosity drops by roughly 10 orders of magnitude (Fig. 3a), before returning to its background value shortly after the end of each seismic event. Long-term histories of fluid pressure on the fault indicate that, for the given hydraulic properties, fluid-pressure cycles are regular and most importantly driven by local pressure gradients (Fig. 3b). However, compared to the viscosity, while the rapid increase in fluid pressure is largely recovered shortly after the end of each event, a significant fraction of it decreases over a longer timescale due to pore pressure diffusion (Fig. 3a).

In our model, earthquakes nucleate due to a coupled strain mechanism between the porous (solid) matrix and pore-fluid. While the rate-

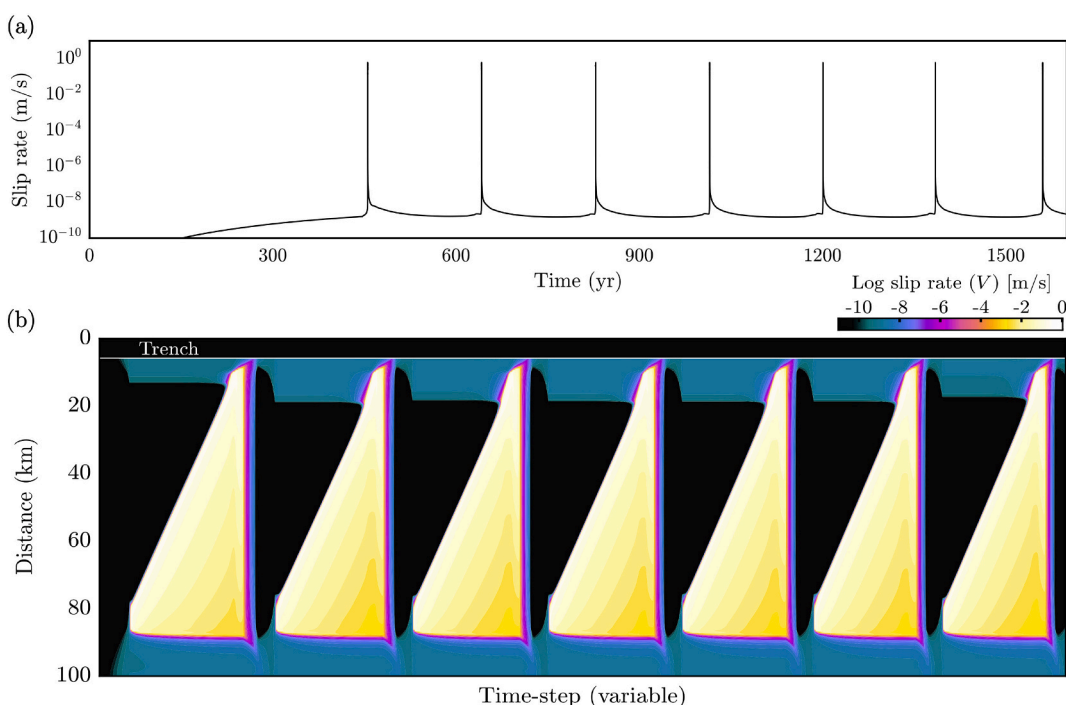


**Fig. 2.** Overview of the modeling results with a constant permeability distribution. (a) Temporal evolution of the maximum slip velocity on the megathrust. Slip rate on the megathrust varies 9 orders of magnitudes from the interseismic periods to the coseismic phase of dynamic rupture. (b) Long-term histories of slip rate on the megathrust, which display a pattern of quasi-periodic complete ruptures. Note that, in order to visualize the evolution of dynamic ruptures, the x-axis displays the time step. The simulation periods are 1600 years, which start with an initial spin-up period of  $\sim 400$  years. Slip rate is plotted on the logarithmic scale.

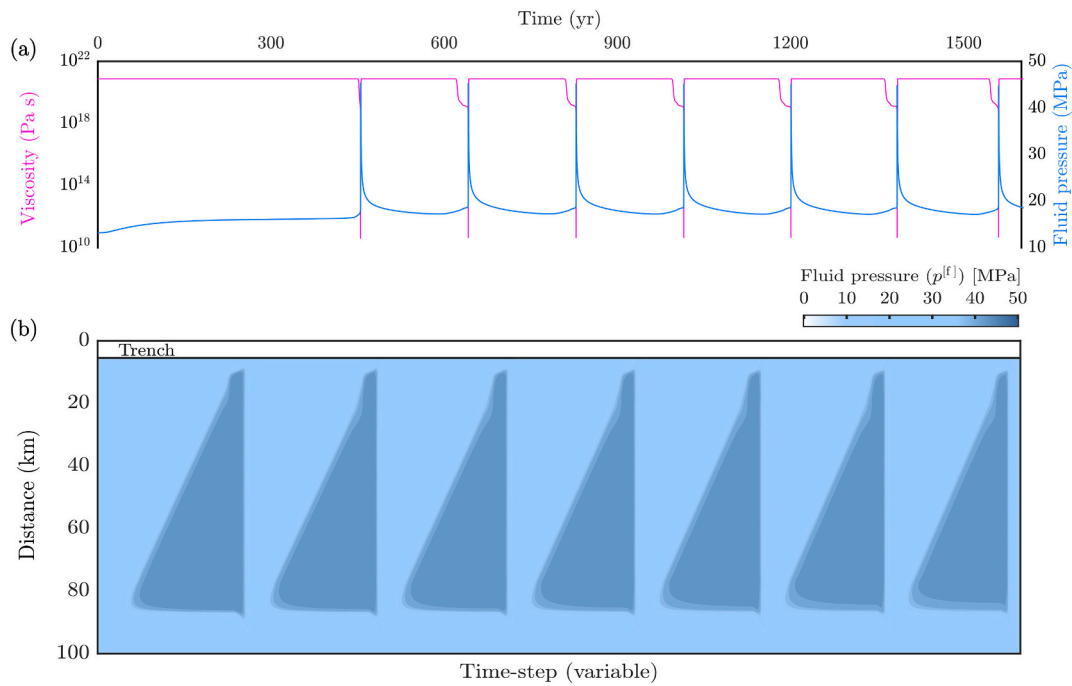


**Fig. 3.** Overview of fluid pressure and viscosity evolution on the megathrust for the model with a constant permeability distribution. (a) Temporal evolution of pore pressure and viscosity in the seismogenic zone. Dynamic ruptures are associated with an increase of fluid pressure and a significant reduction of viscosity. (b) Long-term evolution of fluid pressure shows a pattern of pore-fluid pressure cycling. For the given permeability on the fault, fluid pressure rapidly increases during the nucleation and propagation of earthquakes, and drops a lower level after each event. To visualize the evolution of dynamic ruptures, which occurs in a few seconds, the  $x$ -axis displays the time step.

strengthening rheology allows the fault to slowly accelerate up to its critical nucleation patch for slip to become unstable (Fig. 4a), the viscosity slowly decreases due to strain rate localization (Fig. 4b). As yielding proceeds, the nucleation patch expands up to its critical nucleation length and a dynamic rupture begins (Fig. 4a). Localized strain is associated with the collapse of pores and visco-plastic compaction of the fault zone (Fig. 4c), which is instantaneously counteracted by a negative increase (i.e., expansion) of fluid decompaction (Fig. 4d). This mechanism is highly efficient as it leads to a dynamic self-pressurization of fluids inside the low permeable fault zone, which in turn causes shear strength weakening and the propagation of a dynamic rupture in the form of a pulse-like pore-pressure wave (Fig. 4c, d). For the given permeability on the fault, the timescale of fluid pressurization is much shorter than the timescale of pore-pressure diffusion, building to undrained conditions that are more favorable to failure.

Notably, our simulated fluid-driven dynamic ruptures display some qualitative similarities with seismic cycle models where the dynamic weakening is instead controlled by rate- and state-dependent friction (e.g., Barbot, 2019; Lapusta et al., 2000). The average slip rate is  $0.91 \text{ m s}^{-1}$  and the average rupture speed indicates that fluid-driven dynamic ruptures propagate at  $\sim 2.78 \text{ km s}^{-1}$ , below the shear wave speed (sub-Rayleigh regime). Our models also indicate that fluid-driven shear ruptures become unstable when they reach the critical nucleation length ( $L_c$ ) proposed by Andrews (1976), in which shear strength linearly decreases from static shear strength ( $\tau_s$ ) to a relatively low dynamic shear strength ( $\tau_d$ ) over a characteristic slip weakening distance ( $d_c$ ) (Ida, 1972)

$$L_c = \frac{\mu (\tau_s - \tau_d) d_c}{\pi (1 - \nu) (\tau_0 - \tau_d)^2}, \quad (11)$$

where  $\tau_0$  represents the initial shear stress from the Drucker-Prager-type yield criterion (Eq. (3)). According to our model, Eq. (11) predicts a critical nucleation length of  $\sim 6.7 \text{ km}$  (Fig. 4a). It is critical to note that, in our model, the characteristic slip weakening distance  $d_c$  is treated as

variable and it may dynamically change from one event to another based on the shear stress and pore-pressure level. This is in contrast with rate-and-state friction models where  $d_c$  is often imposed as a constant (e.g., Ben-Zion and Rice, 1995; Lapusta et al., 2000; Lapusta and Liu, 2009; Rubin and Ampuero, 2005; Tse and Rice, 1986).

Laboratory experiments exhibit the well-known increase in strength with the logarithm of time since the last slip episode (Dieterich, 1972). Recent constraints on changes in fault properties suggest that the effective weakening distance may vary over time depending on slip history and loading conditions (e.g., Beeler et al., 2022; Guatteri et al., 2001; Tinti et al., 2004), and observations also suggest that  $d_c$  should be treated as a variable (Cocco and Bizzarri, 2002; Nielsen et al., 2010). In our numerical experiments,  $d_c$  may vary between 1 and 3 m depending on the stress and pore-pressure level in the nucleation region. Although this range of  $d_c$  is substantially larger than typical values adopted for rate-and-state friction models (e.g., Lapusta et al., 2000), our values of  $d_c$  resemble those inferred in rotary friction experiments performed at seismic slip rates ( $\sim 1 \text{ m s}^{-1}$ ), which predict weakening distances of the order of meters (Nielsen et al., 2016a, and references therein), substantial friction drops (Di Toro et al., 2011), and fracture energies of the same order as those inferred from seismological estimates (Nielsen et al., 2016b).

We then analyze the slip history on the fault by assessing whether the maximum slip velocity exceeds the following coseismic velocity threshold ( $V_{th}$ )

$$V_{th} = \frac{2 \gamma p_{eff} c_s}{\mu}, \quad (12)$$

where  $p_{eff}$  is the effective pressure ( $p_{eff} = p^{[t]} - p^{[f]}$ ) and  $c_s$  is the shear wave speed (see Table 1). According to our parameters, Eq. (12) yields a threshold of  $9.1 \text{ cm s}^{-1}$ . The spatiotemporal evolution of the cumulative slip over multiple earthquake cycles displays interseismic periods every 5 yr interval, aseismic slip transients ( $V_p < V < V_{th}$ ), and the coseismic slip every 1 s interval when the maximum slip velocity exceed the

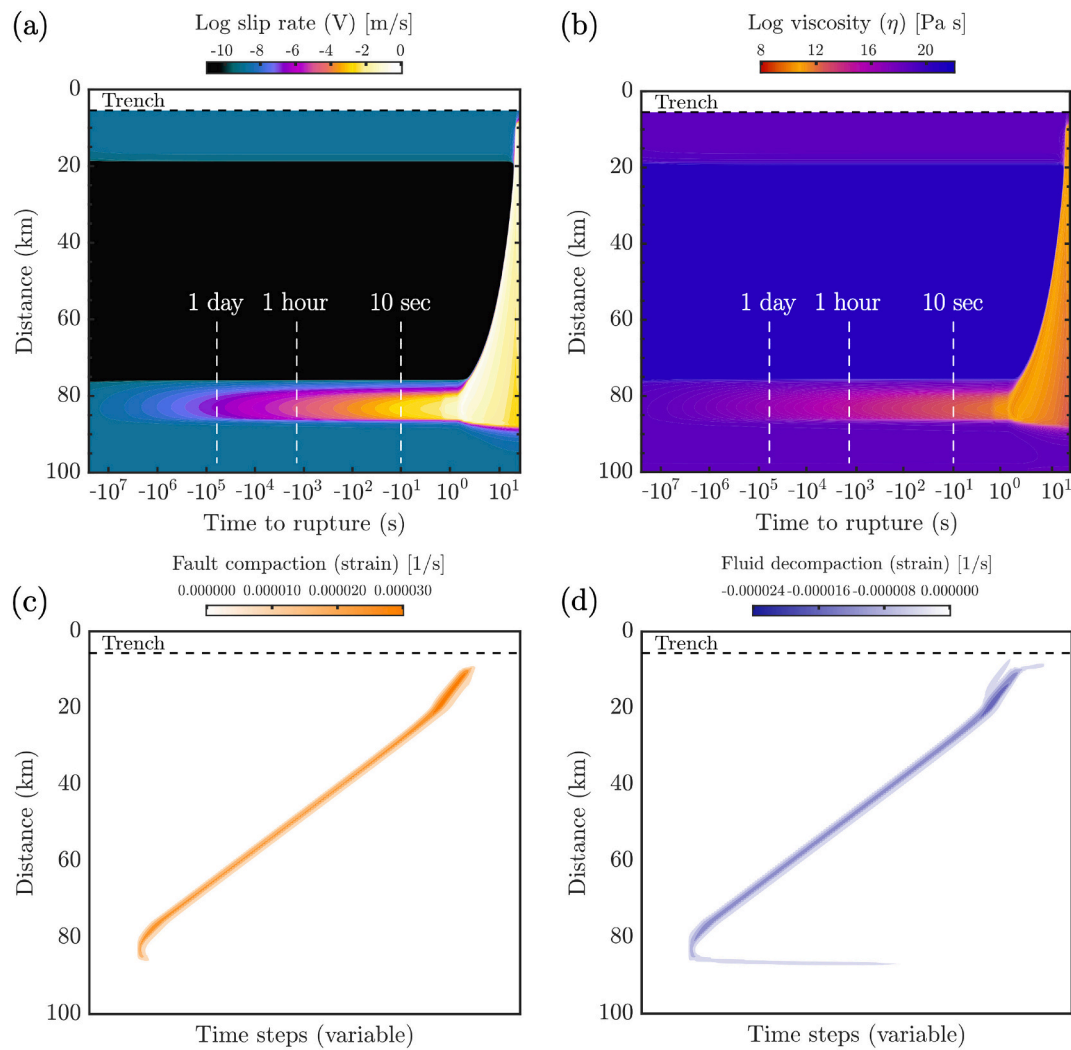


**Fig. 4.** Creep acceleration leading up to a complete megathrust rupture. (a) Slip velocity across the entire fault vs. the logarithmic of the time prior to the beginning of the rupture. Note the slow acceleration of slip rate and the sudden acceleration in nearby creeping patches and the widening of the fast-slipping event. (b) Slow viscosity reduction during the nucleation phase and successive viscosity drop during the propagation of the seismic rupture. (c) Fault compaction and (d) fluid decompaction during the nucleation and propagation of the same event display the governing mechanism that allows seismic events to propagate in the form of solitary pore-pressure waves. In this case, the  $x$ -axis displays the time step.

velocity threshold (Fig. 5). It is interesting to note that dynamic ruptures propagate as solitary pore-pressure waves in the form of sharp pulse-like ruptures (Fig. 4c, d). However, the cumulative slip captures a long tail of low coseismic slip (Fig. 5), suggesting that fluid-driven megathrust ruptures propagate mainly as mild crack-like ruptures (Lambert et al., 2021). Although the long-term fault behavior of the presented model shows similar features of earthquake recurrence and size, it does not produce characteristic earthquakes, nor does it obey the slip-predictable or the time-predictable behavior at a given point on the megathrust. The model does not exhibit the time-predictable behavior because it does not incorporate a fixed threshold of static shear strength ( $\tau_s$ ) for slip to occur. However, since this model displays regular cycles of complete ruptures, the long-term behavior is closer to being slip predictable. This is because, after each complete rupture, the shear stress drops to a low and comparable level throughout the seismogenic zone, approximately determined by the increase of pore-pressure at coseismic slip rates.

### 3.2. Depth-varying permeability

We then consider a depth-varying permeability (Fig. 1c), which is used to mimic a plate interface acting as a low permeability seal. Modeling results indicate that the presence of a low-permeability zone

significantly affect the slip response of the megathrust (Fig. 6). During the interseismic periods, the low permeability zone reduces fluid mobility — particularly in the fault segment where most of the seismic events nucleate — thus promoting a faster self-pressure of pore-fluid inside the undrained fault zone. As a result, the recurrence time of seismic ruptures becomes shorter than the model with homogeneous hydraulic properties (Fig. 6a). Notably, the premature nucleation of seismic ruptures fuels the emergence of partial and complete ruptures on the megathrust (Fig. 6b). Although the megathrust is fully locked during the interseismic periods, a sequence of partial ruptures systematically precede full ruptures. While most of the partial ruptures nucleate and propagate only in the lower edge of the interseismically locked megathrust, up-dip aftershocks occasionally nucleate shortly after a partial rupture (Fig. 6b). Aftershocks typically nucleate in the arrested zone of the previous partial rupture, and propagate both up-dip to the trench and down-dip, re-rupturing part of the fault segment unzipped by the partial rupture (Fig. 6b). Complete ruptures tend to have similar size and recur quasi-periodically every 350–400 years. Between them, a range of smaller events occurs, which release only a small fraction of the accumulated strain.

In combination with the low permeability zone, this leads to overpressures and to a dynamic and heterogeneous environment where the

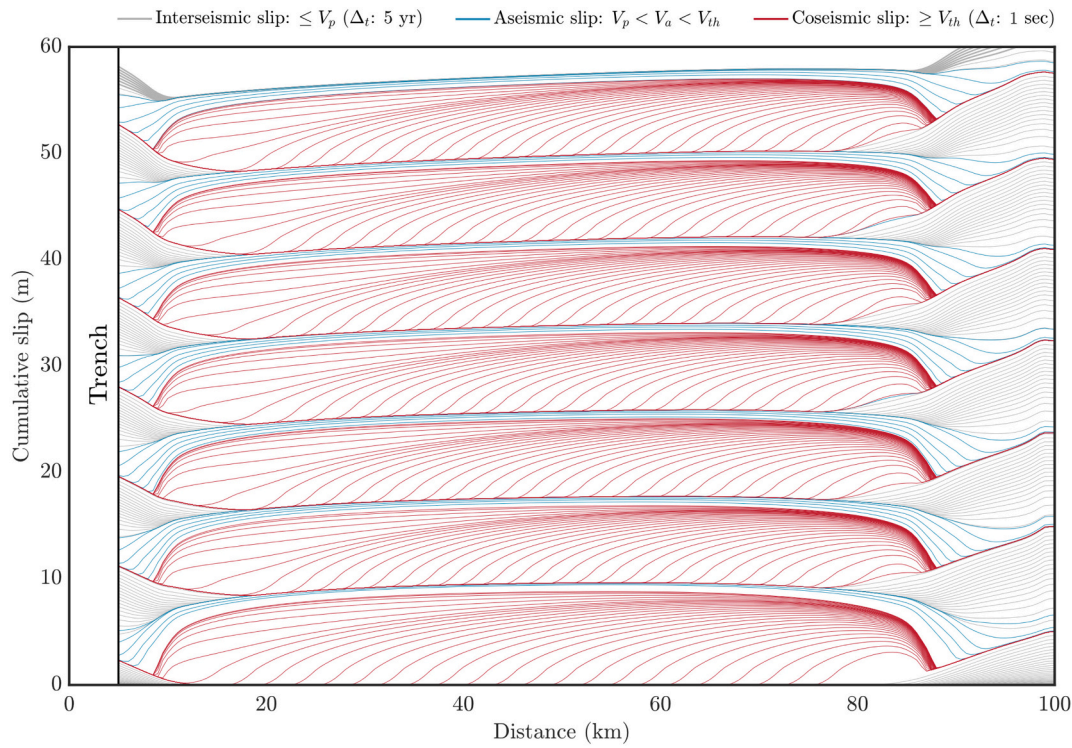


**Fig. 5.** Cumulative slip on the megathrust after multiple events. Red lines indicate the coseismic slip every 1 s interval when the maximum slip velocity exceeds the threshold ( $V_{th}$ ) of  $0.091 \text{ m s}^{-1}$  (Eq. 12). Gray lines (every 5 yr interval) illustrate the interseismic (aseismic) behavior on the fault, whereas the blue lines indicate the aseismic slip transients ( $V_p < V < V_{th}$ ). (For interpretation of the references to colour in this figure legend, the reader is referred to the web version of this article.)

lower edge of the active megathrust is associated with slow fluid expulsion (Fig. 6c) due to the relationship between fault permeability and Darcy flux ( $q$ )

$$q = -\frac{k^{[\phi]}}{\eta^{[f]}} \nabla p^{[f]}, \quad (13)$$

where  $k^{[\phi]}$  is the porosity-dependent permeability and  $\eta^{[f]}$  is the dynamic fluid viscosity. Thus the distribution of permeability exerts fundamental controls on fluid pressure cycling. Our modeling results demonstrate that fault zone architecture controls the long-term pattern of fluid pressure and provides direct evidence that non-constant fault permeability is synchronous with irregular seismic activities characterized by small and large events (Fig. 6c). Transiently elevated fluid pressure in the fault zone also highlights that the sensitivity of permeability to effective stress can give rise to solitary pore-pressure waves (Rice, 1992). In particular, our conceptual model indicates that subduction margins characterized by low-permeability rocks should be poorly drained and highly prone to fluid pressurization and transient fault weakening.

When only the downdip edge of the locked zone is unzipped, stress is transferred to the neighbouring updip region by a static stress transfer and the coseismic slip is of the order of 4–5 m (Fig. 7). Typically the next partial rupture nucleates even sooner than the previous event (Fig. 6a), with the new rupture being generally larger than the previous one. Stress increases in the frontal part of the megathrust, while the ongoing tectonic loading increases the slip deficit throughout the megathrust. Once the stress level is high on the entire seismogenic zone, a complete event eventually propagates through the whole fault system. Notably, during the propagation of complete ruptures, the downdip segment typically results in 4–5 m of coseismic slip, whereas the shallower segment of the megathrust generates a larger coseismic slip of 8–9 m due to a larger slip deficit (Fig. 7). Following the complete rupture, an initial period of quiescence is followed by a new cycle of partial ruptures.

### 3.3. Seismic and aseismic slip spectrum: permeability vs. porosity

Based on the reference models, we conduct a parameter study to investigate how permeability and porosity on-fault affect the transition between regimes in the slip spectrum, from seismic to aseismic slip. In this parameter study, we keep all physical model parameters fixed and we systematically change only porosity and permeability. Note that the effective permeability ( $k^{[\phi]}$ ) depends on the porosity itself and is computed as

$$k^{[\phi]} = k^* \left( \frac{\phi}{\phi^*} \right)^n, \quad (14)$$

where  $k^*$  and  $\phi^*$  are the reference permeability and reference porosity (Table 1), respectively, and  $n$  is a porosity-dependent exponent, which for natural pores is assumed to be 3 (Connolly and Podladchikov, 2000; Rice, 1992), and implies that permeability changes as a cube of increasing porosity.

By varying the hydraulic properties on the fault, we assess whether the maximum slip velocity exceeds the coseismic velocity threshold ( $V_{th}$  – Eq. (12)). Our numerical results predict the emergence of a broad slip spectrum characterized by four main regimes (Fig. 8a): seismic events (Fig. 8b), slow-slip events (Fig. 8c), decaying oscillations (Fig. 8d), and aseismic creep (Fig. 8e). Seismic events occur for a broad range of permeability and porosity, and the recurrence time primarily depends on the permeability value. Relatively higher values of permeability yield regular cycles of large events, whereas lower permeability values lead to the emergence of complex aperiodic periods characterized by small and large events. For lower values of permeability we observe a transition from seismic events to slow-slip events (Fig. 8c), in which the slip rate accelerates up to  $\sim 10^{-5}\text{--}10^{-4} \text{ m s}^{-1}$ , but the slip does not evolve into a dynamic instability. When assuming even lower values of permeability, the slip response on the fault is characterized by decaying oscillations towards stable sliding, where the amplitude of slip transients decay with time until the fault steadily slips at the loading slip velocity. Decaying

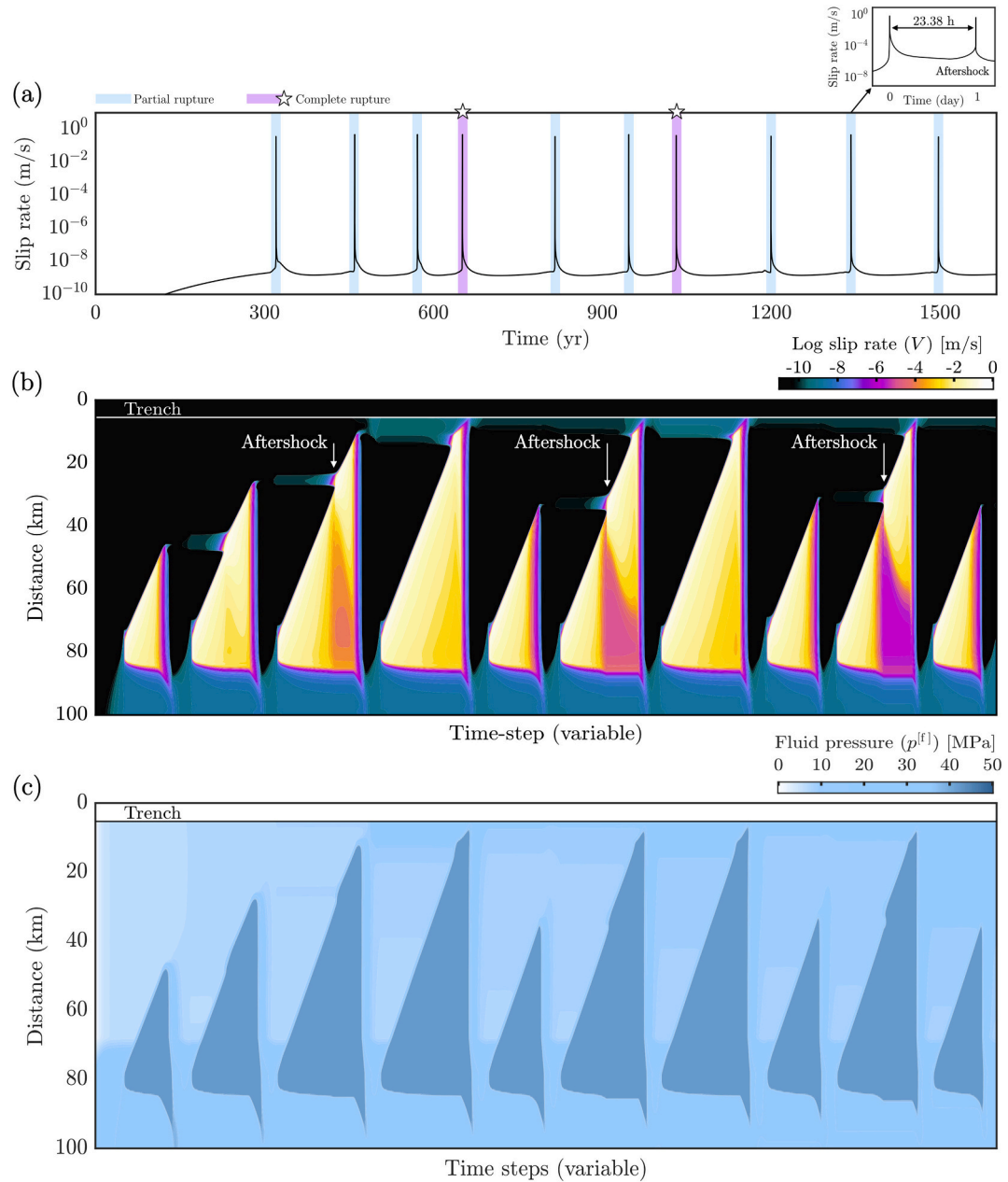


**Fig. 6.** Overview of slip velocity and fluid pressure on the megathrust for the model with a depth-dependent permeability distribution. (a) Temporal evolution of the maximum slip velocity on the megathrust, which displays the temporal evolution of partial and complete ruptures. The small inset shows the short time period separating a partial rupture and a shallow aftershock. (b) Long-term histories of slip rate on the megathrust showing the aperiodic pattern characterized by small and large events. (c) Long-term pattern of fluid pressure on the fault, which highlights the fluid pressure increase during seismic events and a downdip increase of fluid pressure due to a depth-dependent permeability distribution. The x-axis displays the time step.

oscillations emerge because fluid pressurization occurs prematurely, even when the stress state on- and off-fault is low. The slip velocity of these events is thus low and the interseismic periods are relatively short. As a result, the stress level remains low, while the fluid pressure on-fault increases after each event up to a level where the effective pressure is close to zero and the fault steadily slips at the loading slip.

When increasing the porosity, the parameter space in which we identify the transition between seismic and aseismic events shifts towards higher values of permeability (Fig. 8a). However, the transition for low and high permeabilities follow different scaling relationships due to the different predominant mechanisms. For relatively low permeability values, the transition between seismic and aseismic slip predicts the scaling relation from Eq. 14, in which porosity and permeability follows a cubic scaling ( $k^{[\phi]} \propto \phi^3$ ). On the other hand, for

relatively high permeability values, the parameter space in which we observe seismic events strongly depends on the porosity, particularly for  $\phi$  between 1 and 4%. This effect occurs because any small change in porosity causes an increase in the poroelastic properties, including the storage capacity ( $\beta^*$ ) and the drained compressibility ( $\beta^{[d]}$ )

$$\beta^* = \phi (\beta^{[f]} - \beta^{[s]}) + (\beta^{[d]} - \beta^{[s]}), \quad (15)$$

$$\beta^{[d]} = \frac{1}{(1-\phi)} \left( \frac{1}{K^{[\phi]}} + \frac{1}{\beta^{[s]}} \right)^{-1}, \quad (16)$$

where  $\beta^{[f]}$  is the compressibility of the fluid phase,  $\beta^{[s]}$  is the compressibility of the solid matrix, and  $K^{[\phi]}$  the effective bulk modulus of pores. The higher the porosity, the higher the compressibility of pores.

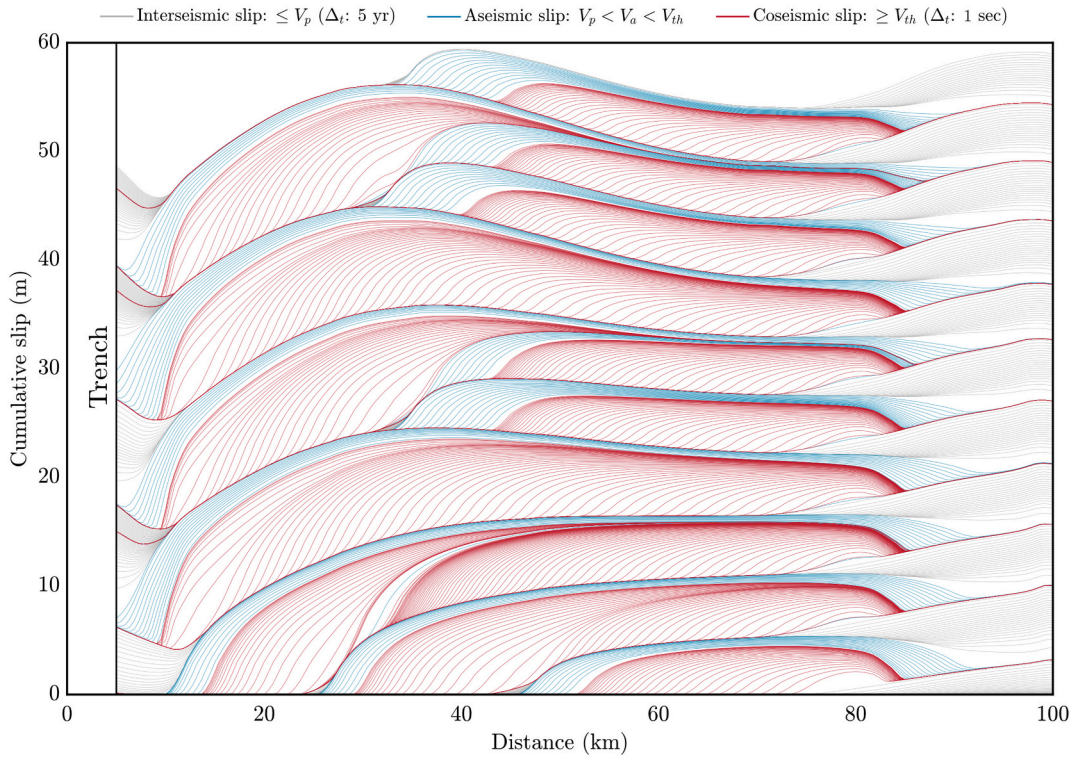


**Fig. 7.** Cumulative slip on the megathrust model with a depth-dependent permeability after multiple partial and complete events. Red lines indicate the coseismic slip every 1 s when the maximum slip velocity exceeds the threshold ( $V_{th}$ ) of  $0.091 \text{ m s}^{-1}$  (Eq. (12)). Gray lines (every 5 yr) illustrate the interseismic (aseismic) behavior on the fault, whereas the blue lines indicate the aseismic slip transients ( $V_p < V < V_{th}$ ). Note that the depth-dependent permeability leads to partial ruptures and substantial aseismic within the seismogenic zone, which often precede the occurrence of shallow aftershocks. (For interpretation of the references to colour in this figure legend, the reader is referred to the web version of this article.)

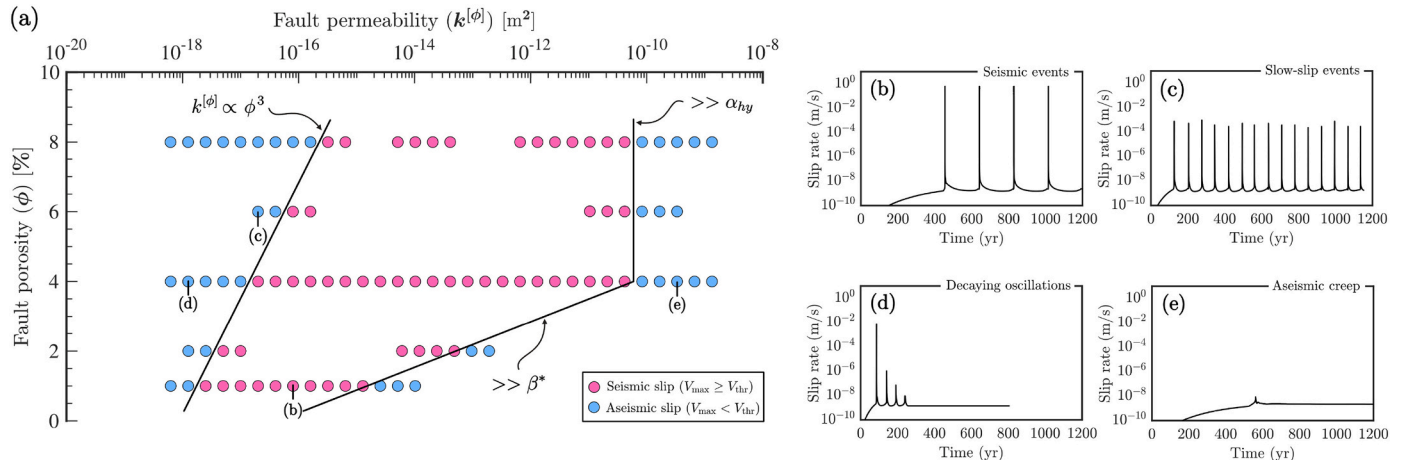


**Fig. 8.** Slip spectrum as a function of the different fault permeability ( $k^{[\phi]}$ ) and fault porosity ( $\phi$ ). (a) Slip spectrum is expressed as the maximum slip velocity ( $V_{\max}$ ) with respect to the slip velocity threshold ( $V_{th}$ ) of  $0.091 \text{ m s}^{-1}$  (Eq. (12)). Four main regimes are identified: (b) seismic events, (c) slow-slip events, (d) decaying oscillations towards stable sliding, and (e) aseismic slip. For low permeability values, the transition from seismic to aseismic follows a cubic scaling between permeability and porosity ( $k^{[\phi]} \propto \phi^3$ ). For high permeability values, the transition from seismic to aseismic strongly depends on the porosity, which controls the poroelastic properties and the storage capacity ( $\beta^*$ ). For high permeability and high porosity ( $\geq 4\%$ ), the hydraulic diffusivity ( $\alpha_{hy}$ ) increases significantly and the fault response is dominated by pore-pressure diffusion, rather than fluid pressurization.

As a result, an increase in porosity leads to a larger compaction of the fault zone and pore-fluid pressurization on-fault can occur for relatively higher values of permeability (Fig. 8a).

For porosity between 4 and 8%, our results indicate that seismic events do not occur for permeability values larger than  $\sim 10^{-10} \text{ m}^2$ . These results highlight the competing effect between pore compressibility and hydraulic diffusivity ( $\alpha_{hy}$ ), which relates the permeability

( $k^{[\phi]}$ ) and storage capacity ( $\beta^*$ ) in the following way:

$$\alpha_{hy} = \frac{k^{[\phi]}}{\eta^{[r]} \beta^*} . \quad (17)$$

According to our results, fluid pressurization strongly depends on the hydraulic diffusion length ( $L$ ), which is related to the hydraulic diffusivity as (Lachenbruch, 1980):

$$L(t) = \sqrt{4 \alpha_{hy} t} . \quad (18)$$

This hydraulic diffusion length gives an estimate of the location of the fluid pressure front over time for such type of diffusion problem (Carslaw and Jaeger, 1959). Our models capture that favorable conditions for the propagation of seismic events arises when fluid pressurization is faster than the hydraulic diffusion. For porosity >4%, our space parameter displays a permeability threshold after which no seismic events can nucleate, thus making the fault system dominated by pore pressure diffusion under drained conditions. This simple principle suggests that the hydraulic properties, which control the onset of pore-pressure pulses, are likely the governing parameters controlling the nucleation and propagation of slow- and fast rupture in the form of pore-pressure waves.

## 4. Discussion

### 4.1. Dynamic influence of fluids on seismic and aseismic slip

Over the last decades, observations from several plate boundary megathrust faults have provided growing evidence for a systematic depth-dependence of seismic and aseismic slip behavior (e.g., Bilek and Lay, 2018; Bürgmann, 2018; Jolivet and Frank, 2020; Lay et al., 2012; Peng and Gomberg, 2010). Downdip variations in rock rheology (e.g., Heuret et al., 2012; Huang et al., 2012; Noda and Lapusta, 2013), fault geometry (e.g., Bleiter et al., 2016; Wang and Bilek, 2011), temperature (e.g., Avouac, 2015; Blanpied et al., 1991; Hyndman and Wang, 1993; Sibson, 1982), and pore-fluid pressure (e.g., Saffer and Tobin, 2011) have often been invoked to explain such depth-dependence of slip behavior along megathrust faults. More recently, a number of studies have provided compelling evidence that earthquake source processes may be controlled by the effect of fluids that permeate the Earth's crust (e.g., Bilek and Lay, 2018; Saffer and Tobin, 2011). Fluids escaping from the oceanic crust and sediments reduce the effective pressure along the plate interface and play an integral role throughout the earthquake cycles (e.g., Miller, 2013), destabilize creeping fault segments (e.g., Noda and Lapusta, 2013), and facilitate the occurrence of slow-slip events (e.g., Dal Zilio et al., 2020a; Liu and Rice, 2007; Segall et al., 2010).

While numerical models often treat pore-fluid pressure as a constant quantity, a growing body of evidence have documented fluctuations in pore-fluid pressure and unsteady fluid migration along faults (e.g., Audet and Bürgmann, 2014; Audet and Schaeffer, 2018; Gao and Wang, 2017; Kodaira et al., 2004; Sibson, 1990). One of the most compelling examples have been documented in the Mexican subduction zone, where variations in the rate of low-frequency earthquakes recorded by Global Positioning System (GPS) seem to be caused by transient changes of pore-fluid pressure over month-long time scales (Frank et al., 2015). Furthermore, earthquake focal mechanisms recorded on an ocean-bottom seismic network from the northern Hikurangi subduction zone indicate that the principal compressive stresses systematically decreases before slow-slip events and subsequently increases during the evolution of each slow-slip event, suggesting that stress and pore-fluid pressure on the megathrust evolve before and during slow-slip events (Warren-Smith et al., 2019). These observations have important implications regarding the role of fluid flow and pore pressure evolution on faults, as they suggest that pore-fluid pressure is a dynamic quantity that do not only passively weaken the plate interface but also play an active role in earthquake source processes over earthquake cycle timescales. The episodicity of pore-fluid pressure fluctuation — which may influence the timing of slow and fast slip — is likely very important near the base of the seismogenic zone, where other processes are simultaneously active, such as brittle-plastic deformation with layers of foliated cataclasite (Angiboust et al., 2015), tectonic underplating (Menant et al., 2019), stacking of shear zones (Delph et al., 2021), silica deposition (Audet and Bürgmann, 2014), and serpentization (Wada et al., 2008).

### 4.2. Evidence of fluids modulating the strength of faults

An essential aspect of understanding the role of fluids and viscous deformation in controlling slow and fast slip events comes from exhumed rocks, which are exposed in a wide range of subduction complexes (Behr and Bürgmann, 2021). Observations thus far suggest that rocks from the source depths of slow-slip events and tremors preserve both long-term strain — accumulated over millions of years — as well as episodic deformation in which fluids are abundant and fluid pressures are near-lithostatic. On the one hand, at geologic timescales, deformation is accommodated by viscous flow in the weaker units of the megathrust, involving both pressure solution and dislocation creep (Calvert et al., 2020; Wassmann and Stoeckert, 2013). On the other hand, at shorter timescales, one of the most widely documented potential markers of transient deformation on subduction megathrusts are *mélange belts*, which are generally defined as blocks of highly viscous material embedded in a less viscous matrix characterized by localized strain (Cloos, 1982; Raymond, 1984). The brittle deformation of these clasts has been associated with stress concentrations, pressure solution and dilatational micro-cracking (Den Hartog and Spiers, 2014; Fagereng and Den Hartog, 2017), and by episodic increases in pore-fluid pressures (Beall et al., 2019; Reber et al., 2014). In that regard, the presence of abundant veins of quartz is a proxy for tensile fractures, which require the pore fluid pressures to locally exceed the magnitude of the minimum compressive stress (Cox, 2010; Sibson, 1998). In particular, these extensional veins are often oriented at high angles compare to the shear fabric, which imply lithostatic pore-fluid pressures and low differential stresses, while the presence of “crack-seal” textures are indicators of pulses of episodic precipitation (Fagereng et al., 2010; Muñoz-Montecinos et al., 2021; Ramsay, 1980).

The emergence of aperiodic sequences characterized by partial and complete megathrust ruptures is commonly interpreted as being the result of heterogenous loading of the seismogenic zone region during the interseismic periods (e.g., D'Acquisto et al., 2020; Dal Zilio et al., 2019; Qiu et al., 2016). The downdip limit of the seismogenic zone is often affected by a stress concentration due to the velocity-weakening to velocity-strengthening transition and due to a faster rate of re-loading than the central region, making that fault segment boundary a preferential site for earthquake nucleation (e.g., Barbot, 2019). The velocity-weakening to velocity-strengthening behavior at depth is responsible for locked-to-creeping transition of the megathrust, which causes stress concentration (e.g., Dal Zilio et al., 2022b). According to our model, such stress concentration is non-stationary in space and time. For example, Fig. 6 shows that, during the interseismic periods, creep migrates updip from the velocity-strengthening region to the seismogenic zone, leading to a mechanical erosion of the lower edge of the locked patch. The extent of this temporary unlocked segment of the fault is comparable to the critical nucleation length ( $L_c$ ) computed from Eq. (11) (Fig. 4a). In nature, small events or partial ruptures appear in the vicinity of the deep transition between the locked and the creeping regions (e.g., Jiang and Lapusta, 2016), and this region is often interpreted as the source of dominant high-frequency radiation due to high pre-seismic shear stress (e.g., Michel et al., 2017). Furthermore, pulse-like ruptures — which are often observed in various tectonic settings (Heaton, 1990) — can form as a result of the stress concentration at the boundary between velocity-weakening to velocity-strengthening, or at any other band of concentrated stress. Dynamic ruptures that nucleate near the downdip edge of the seismogenic zone and propagate up to the trench can encounter regions of lower stresses and may therefore arrest within the locked region (Lapusta and Rice, 2003; Rice, 1993; Wu and Chen, 2014). In our simulations, an increasing complexity in fault dynamics is associated with dynamic pore-fluid pressure changes and the hydraulic properties on-fault. Assuming a depth-dependent permeability predicts aperiodic sequences of partial and complete megathrust ruptures, fluid-driven aseismic slip, and shallow aftershocks, which arise as over-pressure pulses migrating upward along the megathrust. Large events

typically accompany fluid-driven postseismic slip, which occur both at rupture edges and within the ruptured segment.

Fluid pressurization as a dominant mechanism leading to fault failure and earthquake propagation has already been reported by a number of studies. Numerical experiments suggest that thermal pressurization of pore fluids trapped in the fault zone can reduce the dynamic shear strength of faults during seismic slip (Rice, 2006; Sibson, 1973). The combination of low dynamic fault strength and short weakening distances enables rupture propagation in shallow sections of the megathrust and also promotes large seismic slip (Noda and Lapusta, 2013). Laboratory measurements of pore-fluid pressure variations during fast slip in fault gouge samples seem to confirm theoretical studies, highlighting that both mechanical compaction and fluid pressurization can overcome the initial phase of shear-induced dilatancy and thus induce fault failure (Aretusini et al., 2021). The key novelty of our modeling approach lies on the fact that dynamic pore-pressure variations may control the effective stress on the megathrust and thus the fault strength, without requiring any additional rate-weakening friction law. A critical condition for the propagation of pore-pressure waves is the existence of pressure gradients in the fault zone. According to our results, pressure gradients result from the compaction of the fault zone and localized strain (Fig. 4). Another critical condition for the propagation of pore-pressure waves is governed by the competition between pore-fluid pressurization and pore-pressure diffusion. When the timescale of fluid pressurization is shorter than pore-pressure diffusion, fluids can efficiently pressurize and thus trigger a dynamic instability. Conversely, when pore-pressure diffusion is faster or comparable to fluid pressurization, fast fluid expulsion prevent fluid pressurization and the propagation of pore-pressure waves. To this end, depending on the hydraulic properties (Fig. 8), our models predict the full spectrum of seismic and aseismic slip including seismic events, slow-slip events, oscillatory decay with time, and stable aseismic creep. Our findings have strong implications, as they demonstrate that dynamic self-pressurization of pore-fluid and the propagation of pore-pressure waves are likely governing mechanisms controlling fast- and slow-slip events on the plate interface of subduction megathrusts.

#### 4.3. Modeling limitations

Despite a simplified model setup, our hydro-mechanical earthquake cycle models demonstrate the ability to capture a rich variety of seismic processes. However, we recognize that in order to make a full comparison to subduction megathrust in geological settings we need to understand how the reported fluid-driven instabilities manifest in three dimensions (e.g., Jiang et al., 2022). Inelastic changes of porosity and permeability, which can arise from fractures (e.g., Rutqvist, 2015), shear-induced dilatancy (e.g., Segall and Rice, 1995), temperature-dependent rock (de)hydration (e.g., Poulet et al., 2014), and mineral precipitation in pores (e.g., Renard et al., 2000; Tenthorey et al., 2003), have been neglected for simplicity. However, our results demonstrate that the (de)compaction of the fault zone and associated fluid pressurization is the dominant mechanism controlling the occurrence of fault instability. Shear-induced dilatancy of fault gouge is a transient phenomenon during the initial stages of the slip, and its effect is poorly constrained at great depth as it is only investigated experimentally at relatively low-pressure conditions (e.g., Brantut et al., 2018). It is likely that this effect will decrease with increasing confining pressure (e.g., Brantut et al., 2018). However, future research will focus on the dynamic evolution of permeability, including deformation-induced changes in pores connectivity, dilatancy effect, as well as the influence of rate- and state-dependent friction and temperature-dependent rock (de)hydration processes in a more complex time-dependent hydro-thermo-mechanical framework.

It is important to note that the model neglects the influence of temperature, which can affect dehydration reactions (e.g., Miller, 2013; Poulet et al., 2014), shear heating and grain size evolution (e.g.,

Thielmann et al., 2015), and thermal pressurization (e.g., Segall and Rice, 2006). Lastly, temperature-dependent (non-Newtonian) rheologies are known to influence the seismic behavior along the subduction interface (Dal Zilio et al., 2022b), especially for the visco-elastic stress build-up and relaxation, which affect the interplay between the long-term tectonic deformation and short-term seismicity (e.g., Dal Zilio et al., 2021; Wang, 2007). In spite of these potential pitfalls, the number of salient yet enigmatic observed features from real subduction megathrusts that our models do succeed in reproducing is highly encouraging and provides useful insights.

#### 5. Conclusions

In summary, we investigate the influence of fluid pressure cycling on seismicity in active megathrust faults based on hydro-mechanical earthquake cycle models. Our findings indicate that the dynamics of solid-fluid interactions on plate boundary megathrust faults can develop a wide range of behaviors based on the hydraulic properties on-fault. Among these, a depth-dependent permeability architecture captures the emergence of complex aperiodic seismic sequences characterized by partial and complete ruptures, as well as aftershocks and transient aseismic slip. Further analysis of the porosity and permeability on the fault reveal that this pair of coupled parameters controls the predominant slip mode on the fault, from seismic events and slow-slip events to decay oscillations and stable creep. Decreasing fault permeability promotes fault pressurization, which translates into the emergence of aperiodic sequences, slow-slip events, and eventually decay oscillations. In contrast, increasing permeability is always associated with higher pore-pressure diffusion, which results in a transition from regular seismic cycles to stable creep for high values of permeability. Porosity controls the poroelastic compressibility on the fault zone. Thus, for higher values of porosity, seismic events can occur even when the fault is more permeable due to an increase in the compaction and associated fluid pressurization. The validity of this behavior relies upon the condition that fluid pressurization due to pore compaction is faster than pore-pressure diffusion. If this is not the case, then pore-fluid cannot pressurize, thus leading to stable creep behavior.

In nature, fault porosity and permeability architecture are poorly constrained and may vary widely from place to place due to their dependence on stress, lithology, temperature, and slip history. The evolution of porosity and permeability and their impact on fluid pathways are much more complex on real faults than have been explored in this study. Nevertheless, the permeability structure adopted in our conceptual model form a convenient phase space to understand fault behavior during all stages of the seismic cycle. Furthermore, our simplified formulation is sufficient to demonstrate the importance of integrating these hydromechanical processes into numerical models, in order to gain a comprehensive understanding of the fluid-rock interaction on active megathrust faults. To this end, our modeling results demonstrate the role of fluid pressure in governing newly observed modes of fault slip, and highlight the need for an improved understanding of the spatial and temporal variability of fault zone permeability, the underlying processes that govern the magnitude and timescales of fluid pressure cycling, as well as the distribution of fluid production and pore pressure in the seismogenic zone.

#### Declaration of Competing Interest

The authors declare that they have no known competing financial interests or personal relationships that could have appeared to influence the work reported in this paper.

#### Acknowledgments

We thank Whitney Behr, David Kammer, Nadia Lapusta, Paul Selvadurai, Antonio Rinaldi, Claudio Petrini, Elias Heimisson, Federico

Ciardo, and Domenico Giardini for discussions. This research was supported by the European Research Council (ERC) Synergy Grant FEAR (ID: 856559). Numerical simulations were performed on ETH cluster Euler. We thank Stephen A. Miller, Laetitia Le Pourhiet, and the Guest Editor Samuel Angiboust for their constructive comments, which helped improve the paper considerably.

## References

- Andrews, D., 1976. Rupture velocity of plane strain shear cracks. *Journal of Geophysical Research* 81 (32), 5679–5687.
- Angiboust, S., Kirsch, J., Oncken, O., Glodny, J., Monié, P., Rybacki, E., 2015. Probing the transition between seismically coupled and decoupled segments along an ancient subduction interface. *Geochemistry, Geophysics, Geosystems* 16 (6), 1905–1922.
- Aretusini, S., Meneghini, F., Spagnuolo, E., Harbord, C., Di Toro, G., 2021. Fluid pressurisation and earthquake propagation in the hikurangi subduction zone. *Nature Communications* 12 (1), 1–8.
- Audet, P., Bürgmann, R., 2014. Possible control of subduction zone slow-earthquake periodicity by silica enrichment. *Nature* 510 (7505), 389–392.
- Audet, P., Schaeffer, A.J., 2018. Fluid pressure and shear zone development over the locked to slow slip region in Cascadia. *Science Advances* 4 (3) eaar2982.
- Audet, P., Bostock, M.G., Christensen, N.I., Peacock, S.M., 2009. Seismic evidence for overpressured subducted oceanic crust and megathrust fault sealing. *Nature* 457 (7225), 76–78.
- Audet, P., Bostock, M.G., Boyarko, D.C., Brudzinski, M.R., Allen, R.M., 2010. Slab morphology in the Cascadia fore arc and its relation to episodic tremor and slip. *Journal of Geophysical Research - Solid Earth* 115 (B4).
- Avouac, J.-P., 2015. From geodetic imaging of seismic and aseismic fault slip to dynamic modeling of the seismic cycle. *Annual Review of Earth and Planetary Sciences* 43, 233–271.
- Barbot, S., 2019. Slow-slip, slow earthquakes, period-two cycles, full and partial ruptures, and deterministic chaos in a single asperity fault. *Tectonophysics* 768, 228171.
- Beall, A., Fagereng, Å., Ellis, S., 2019. Strength of strained two-phase mixtures: Application to rapid creep and stress amplification in subduction zone mélange. *Geophysical Research Letters* 46 (1), 169–178.
- Beeler, N., Rubin, A., Bhattacharya, P., Kilgore, B., Tullis, T., 2022. Apparent age dependence of the fault weakening distance in rock friction. *Journal of Geophysical Research - Solid Earth* 127 (1) e2021JB022772.
- Behr, W.M., Bürgmann, R., 2021. What's down there? The structures, materials and environment of deep-seated slow slip and tremor. *Philosophical Transactions of the Royal Society A* 379 (2193), 20200218.
- Ben-Zion, Y., Rice, J.R., 1995. Slip patterns and earthquake populations along different classes of faults in elastic solids. *Journal of Geophysical Research - Solid Earth* 100 (B7), 12959–12983.
- Bilek, S.L., Lay, T., 2018. Subduction zone megathrust earthquakes. *Geosphere* 14 (4), 1468–1500.
- Biot, M.A., 1941. General theory of three-dimensional consolidation. *Journal of Applied Physics* 12 (2), 155–164.
- Biot, M.A., Willis, D.G., 1957. The Elastic Coefficients of the Theory of Consolidation.
- Bishop, A., 1973. The influence of an undrained change in stress on the pore pressure in porous media of low compressibility. *Geotechnique* 23 (3), 435–442.
- Blanpied, M., Lockner, D., Byerlee, J., 1991. Fault stability inferred from granite sliding experiments at hydrothermal conditions. *Geophysical Research Letters* 18 (4), 609–612.
- Blerty, Q., Thomas, A.M., Rempel, A.W., Karlstrom, L., Sladen, A., De Barros, L., 2016. Mega-earthquakes rupture flat megathrusts. *Science* 354 (6315), 1027–1031.
- Brantut, N., Baker, M., Hansen, L.N., Baud, P., 2018. Microstructural control of physical properties during deformation of porous limestone. *Journal of Geophysical Research - Solid Earth* 123 (6), 4751–4764.
- Bürgmann, R., 2018. The geophysics, geology and mechanics of slow fault slip. *Earth and Planetary Science Letters* 495, 112–134.
- Calvert, A. J., Bostock, M. G., Savard, G., and Unsworth, M. J. (2020). Cascadia low frequency earthquakes at the base of an overpressured subduction shear zone. *Nature Communications*, 11(1):1–10.
- Carlaw, H.S., Jaeger, J.C., 1959. Conduction of Heat in Solids. Technical report. C larendon Press.
- Cloos, M., 1982. Flow melanges: numerical modeling and geologic constraints on their origin in the Franciscan subduction complex, California. *Geological Society of America Bulletin* 93 (4), 330–345.
- Cocco, M., and Bizzarri, A. (2002). On the slip-weakening behavior of rate-and state dependent constitutive laws. *Geophysical Research Letters*, 29(11):11–1.
- Connolly, J., Podladchikov, Y.Y., 2000. Temperature-dependent viscoelastic compaction and compartmentalization in sedimentary basins. *Tectonophysics* 324 (3), 137–168.
- Cox, S., 2010. The application of failure mode diagrams for exploring the roles of fluid pressure and stress states in controlling styles of fracture-controlled permeability enhancement in faults and shear zones. *Geofluids* 10 (1–2), 217–233.
- D'Acquisto, M., Dal Zilio, L., Molinari, I., Kissling, E., Gerya, T., van Dinther, Y., 2020. Tectonics and Seismicity in the Northern Apennines Driven by Slab Retreat and Lithospheric Delamination, 789. *Tectonophysics*, p. 228481.
- Dal Zilio, L., van Dinther, Y., Gerya, T., Avouac, J.-P., 2019. Bimodal seismicity in the Himalaya controlled by fault friction and geometry. *Nature Communications* 10 (1), 48.
- Dal Zilio, L., Lapusta, N., Avouac, J.-P., 2020a. Unraveling scaling properties of slow-slip events. *Geophysical Research Letters* 47 (10).
- Dal Zilio, L., Ruh, J., Avouac, J.-P., 2020b. Structural evolution of orogenic wedges: interplay between erosion and weak décollements. *Tectonics* 39 (10).
- Dal Zilio, L., Hetényi, G., Hubbard, J., Bollinger, L., 2021. Building the Himalaya from tectonic to earthquake scales. *Nature Reviews Earth & Environment* pages 1–18.
- Dal Zilio, L., Hegyi, B., Behr, W., Gerya, T., 2022a. Hydro-mechanical earthquake cycles in a poro-visco-elasto-plastic fluid-bearing fault structure. Preprint arXiv. <https://doi.org/10.48550/arXiv.2201.11786>. <http://arxiv.org/abs/2201.11786>.
- Dal Zilio, L., Lapusta, N., Avouac, J.-P., Gerya, T., 2022b. Subduction earthquake sequences in a nonlinear visco-elasto-plastic megathrust. *Geophysical Journal International* 229 (2), 1098–1121.
- Delph, J.R., Thomas, A.M., Levander, A., 2021. Subcretionary tectonics: linking variability in the expression of subduction along the Cascadia forearc. *Earth and Planetary Science Letters* 556, 116724.
- Den Hartog, S.A., Spiers, C.J., 2014. A microphysical model for fault gouge friction applied to subduction megathrusts. *Journal of Geophysical Research - Solid Earth* 119 (2), 1510–1529.
- Di Toro, G., Han, R., Hirose, T., De Paola, N., Nielsen, S., Mizoguchi, K., Ferri, F., Cocco, M., Shimamoto, T., 2011. Fault lubrication during earthquakes. *Nature* 471 (7339), 494–498.
- Dieterich, J.H., 1972. Time-dependent friction in rocks. *Journal of Geophysical Research* 77 (20), 3690–3697.
- Dieterich, J.H., 1979. Modeling of rock friction: 1. Experimental results and constitutive equations. *Journal of Geophysical Research - Solid Earth* 84 (B5), 2161–2168.
- Dieterich, J., 1981. Constitutive properties of faults with simulated gouge. In: *Monograph 24: Mechanical Behavior of Crustal Rocks*. American Geophysical Union, Washington, DC, pp. 103–120.
- Dieterich, J., 2007. Applications of rate-and state-dependent friction to models of fault-slip and earthquake occurrence. *Treatise on Geophysics* 4, 107–129.
- Faccenda, M., 2014. Water in the slab: a trilogy. *Tectonophysics* 614, 1–30.
- Fagereng, Å., Den Hartog, S.A., 2017. Subduction megathrust creep governed by pressure solution and frictional-viscous flow. *Nature Geoscience* 10 (1), 51–57.
- Fagereng, Å., Remitti, F., Sibson, R.H., 2010. Shear veins observed within anisotropic fabric at high angles to the maximum compressive stress. *Nature Geoscience* 3 (7), 482–485.
- Frank, W.B., Shapiro, N.M., Husker, A.L., Kostoglodov, V., Bhat, H.S., Campillo, M., 2015. Along-fault pore-pressure evolution during a slow-slip event in Guerrero, Mexico. *Earth and Planetary Science Letters* 413, 135–143.
- Gao, X., Wang, K., 2017. Rheological separation of the megathrust seismogenic zone and episodic tremor and slip. *Nature* 543 (7645), 416.
- Gassmann, F., 1951. Elastic waves through a packing of spheres. *Geophysics* 16 (4), 673–685.
- Gerya, T., 2019. Introduction to Numerical Geodynamic Modelling. Cambridge University Press.
- Gerya, T.V., Meilick, F., 2011. Geodynamic regimes of subduction under an active margin: effects of rheological weakening by fluids and melts. *Journal of Metamorphic Geology* 29 (1), 7–31.
- Gerya, T., Yuen, D., 2007. Robust characteristics method for modelling multiphase visco-elasto-plastic thermo-mechanical problems. *Physics of the Earth and Planetary Interiors* 163 (1), 83–105.
- Guatteri, M., Spudich, P., Beroza, G.C., 2001. Inferring rate and state friction parameters from a rupture model of the 1995 Hyogo-ken Nanbu (Kobe) Japan earthquake. *Journal of Geophysical Research - Solid Earth* 106 (B11), 26511–26521.
- Heaton, T.H., 1990. Evidence for and implications of self-healing pulses of slip in earthquake rupture. *Physics of the Earth and Planetary Interiors* 64 (1), 1–20.
- Heimisson, E.R., Dunham, E.M., Almquist, M., 2019. Poroelastic effects destabilize mildly rate-strengthening friction to generate stable slow-slip pulses. *Journal of the Mechanics and Physics of Solids* 130, 262–279.
- Heuret, A., Conrad, C., Funiciello, F., Lallemand, S., Sandri, L., 2012. Relation between subduction megathrust earthquakes, trench sediment thickness and upper plate strain. *Geophysical Research Letters* 39 (5).
- Huang, Y., Meng, L., Ampuero, J.-P., 2012. A dynamic model of the frequency-dependent rupture process of the 2011 Tohoku-oki earthquake. *Earth, Planets and Space* 64 (12), 1061–1066.
- Hyndman, R.D., Wang, K., 1993. Thermal constraints on the zone of major thrust earthquake failure: the Cascadia subduction zone. *Journal of Geophysical Research - Solid Earth* 98 (B2), 2039–2060.
- Ida, Y., 1972. Cohesive force across the tip of a longitudinal-shear crack and Griffith's specific surface energy. *Journal of Geophysical Research* 77 (20), 3796–3805.
- Ikari, M.J., Marone, C., Saffer, D.M., Kopf, A.J., 2013. Slip weakening as a mechanism for slow earthquakes. *Nature Geoscience* 6 (6), 468–472.
- Jiang, J., Lapusta, N., 2016. Deeper penetration of large earthquakes on seismically quiescent faults. *Science* 352 (6291), 1293–1297.
- Jiang, J., Erickson, B., Lambert, V., Ampuero, J.-P., Ando, R., Barbot, S., Cattania, C., Dal Zilio, L., Duan, B., Dunham, E.M., Gabriel, A.-A., Lapusta, N., Li, D., Liu, D., Liu, Y., Ozawa, S., Pranger, C., Van Dinther, Y., 2022. Community-driven code comparisons for three-dimensional dynamic modeling of sequences of earthquakes and aseismic slip (seas). *Journal of Geophysical Research - Solid Earth* 127 (3).
- Jolivet, R., Frank, W., 2020. The transient and intermittent nature of slow slip. *AGU Advances* 1 (1) e2019AV000126.
- Katz, R.F., Spiegelman, M., Holtzman, B., 2006. The dynamics of melt and shear localization in partially molten aggregates. *Nature* 442 (7103), 676–679.
- Kerrick, D., Connolly, J., 1998. Subduction of ophiocarbonates and recycling of CO<sub>2</sub> and H<sub>2</sub>O. *Geology* 26 (4), 375–378.

- Kodaira, S., Iidaka, T., Kato, A., Park, J.-O., Iwasaki, T., Kaneda, Y., 2004. High pore fluid pressure may cause silent slip in the nankai trough. *Science* 304 (5675), 1295–1298.
- Lachenbruch, A.H., 1980. Frictional heating, fluid pressure, and the resistance to fault motion. *Journal of Geophysical Research - Solid Earth* 85 (B11), 6097–6112.
- Lambert, V., Lapusta, N., Perry, S., 2021. Propagation of large earthquakes as self-healing pulses or mild cracks. *Nature* 591 (7849), 252–258.
- Lapusta, N., Liu, Y., 2009. Three-dimensional boundary integral modeling of spontaneous earthquake sequences and aseismic slip. *Journal of Geophysical Research - Solid Earth* 114 (B9).
- Lapusta, N., Rice, J.R., 2003. Nucleation and early seismic propagation of small and large events in a crustal earthquake model. *Journal of Geophysical Research - Solid Earth* 108 (B4).
- Lapusta, N., Rice, J.R., Ben-Zion, Y., Zheng, G., 2000. Elastodynamic analysis for slow tectonic loading with spontaneous rupture episodes on faults with rate-and state-dependent friction. *Journal of Geophysical Research - Solid Earth* 105 (B10), 23765–23789.
- Lay, T., Kanamori, H., Ammon, C.J., Koper, K.D., Hutko, A.R., Ye, L., Yue, H., Rushing, T.M., 2012. Depth-varying rupture properties of subduction zone megathrust faults. *Journal of Geophysical Research - Solid Earth* 117 (B4).
- Liu, Y., Rice, J.R., 2007. Spontaneous and triggered aseismic deformation transients in a subduction fault model. *Journal of Geophysical Research - Solid Earth* 112 (B9).
- Liu, Y., Rubin, A.M., 2010. Role of fault gouge dilatancy on aseismic deformation transients. *Journal of Geophysical Research - Solid Earth* 115 (B10).
- Marone, C., 1998. Laboratory-derived friction laws and their application to seismic faulting. *Annual Review of Earth and Planetary Sciences* 26 (1), 643–696.
- Matsubara, M., Obara, K., Kasahara, K., 2009. High-vp/vs zone accompanying non-volcanic tremors and slow-slip events beneath southwestern Japan. *Tectonophysics* 472 (1–4), 6–17.
- Menant, A., Angiboust, S., Gerya, T., 2019. Stress-driven fluid flow controls long-term megathrust strength and deep accretionary dynamics. *Scientific Reports* 9 (1), 1–11.
- Michel, S., Avouac, J.-P., Lapusta, N., Jiang, J., 2017. Pulse-like partial ruptures and high-frequency radiation at creeping-locked transition during megathrust earthquakes. *Geophysical Research Letters* 44 (16), 8345–8351.
- Miller, S.A., 2013. The role of fluids in tectonic and earthquake processes. In: *Advances in Geophysics*, 54. Elsevier pages 1–46.
- Moresi, L., Dufour, F., Mühlhaus, H.-B., 2003. A lagrangian integration point finite element method for large deformation modeling of viscoelastic geomaterials. *Journal of Computational Physics* 184 (2), 476–497.
- Muñoz-Montecinos, J., Angiboust, S., García-Casco, A., Glodny, J., Bebout, G., 2021. Episodic hydrofracturing and large-scale flushing along deep subduction interfaces: Implications for fluid transfer and carbon recycling (zagros orogen, southeastern Iran). *Chemical Geology* 571, 120173.
- Nielsen, S., Mosca, P., Giberti, G., Di Toro, G., Hirose, T., Shimamoto, T., 2010. On the transient behavior of frictional melt during seismic slip. *Journal of Geophysical Research - Solid Earth* 115 (B10).
- Nielsen, S., Spagnuolo, E., Smith, S., Violay, M., Di Toro, G., Bistacchi, A., 2016a. Scaling in natural and laboratory earthquakes. *Geophysical Research Letters* 43 (4), 1504–1510.
- Nielsen, S., Spagnuolo, E., Violay, M., Smith, S., Di Toro, G., Bistacchi, A., 2016b. G: Fracture energy, friction and dissipation in earthquakes. *Journal of Seismology* 20 (4), 1187–1205.
- Noda, H., Lapusta, N., 2013. Stable creeping fault segments can become destructive as a result of dynamic weakening. *Nature* 493 (7433), 518.
- Peacock, S.A., 1990. Fluid processes in subduction zones. *Science* 248 (4953), 329–337.
- Peng, Z., Gomberg, J., 2010. An integrated perspective of the continuum between earthquakes and slow-slip phenomena. *Nature Geoscience* 3 (9), 599.
- Petrini, C., Gerya, T., Yarushina, V., van Dinther, Y., Connolly, J., Madonna, C., 2020. Seismo-hydro-mechanical modelling of the seismic cycle: Methodology and implications for subduction zone seismicity. *Tectonophysics* 791, 228504.
- Poulet, T., Veveakis, E., Regenauer-Lieb, K., Yuen, D., 2014. Thermo-poro-mechanics of chemically active creeping faults: 3. The role of serpentinite in episodic tremor and slip sequences, and transition to chaos. *Journal of Geophysical Research - Solid Earth* 119 (6), 4606–4625.
- Prager, W., Drucker, D., 1952. Soil mechanics and plastic analysis or limit design. *Quarterly of Applied Mathematics* 10 (2), 157–165.
- Qiu, Q., Hill, E.M., Barbot, S., Hubbard, J., Feng, W., Lindsey, E.O., Feng, L., Dai, K., Samsonov, S.V., Tapponnier, P., 2016. The mechanism of partial rupture of a locked megathrust: the role of fault morphology. *Geology* 44 (10), 875–878.
- Ramsay, J.G., 1980. The crack-seal mechanism of rock deformation. *Nature* 284 (5752), 135–139.
- Raymond, L.A., 1984. Melanges: Their Nature, Origin, and Significance, 198. Geological Society of America.
- Reber, J.E., Hayman, N.W., Lavier, L.L., 2014. Stick-slip and creep behavior in lubricated granular material: Insights into the brittle-ductile transition. *Geophysical Research Letters* 41 (10), 3471–3477.
- Renard, F., Gratié, J.-P., Jamtveit, B., 2000. Kinetics of crack-sealing, intergranular pressure solution, and compaction around active faults. *Journal of Structural Geology* 22 (10), 1395–1407.
- Rice, J.R., 1992. Fault stress states, pore pressure distributions, and the weakness of the San Andreas fault. In: *International Geophysics*, 51. Elsevier pages 475–503.
- Rice, J.R., 1993. Spatio-temporal complexity of slip on a fault. *Journal of Geophysical Research - Solid Earth* 98 (B6), 9885–9907.
- Rice, J.R., 2006. Heating and weakening of faults during earthquake slip. *Journal of Geophysical Research - Solid Earth* 111 (B5).
- Rice, J.R., Ruina, A.L., 1983. Stability of steady frictional slipping. *Journal of Applied Mechanics* 50 (2), 343–349.
- Rubin, A.M., Ampuero, J.-P., 2005. Earthquake nucleation on (aging) rate and state faults. *Journal of Geophysical Research - Solid Earth* 110 (B11).
- Ruina, A., 1983. Slip instability and state variable friction laws. *Journal of Geophysical Research - Solid Earth* 88 (B12), 10359–10370.
- Rutqvist, J., 2015. Fractured rock stress-permeability relationships from in situ data and effects of temperature and chemical-mechanical couplings. *Geofluids* 15 (1–2), 48–66.
- Saffer, D.M., Tobin, H.J., 2011. Hydrogeology and mechanics of subduction zone forearcs: Fluid flow and pore pressure. *Annual Review of Earth and Planetary Sciences* 39, 157–186.
- Schmalholz, S., Podladchikov, Y., Schmid, D., 2001. A spectral/finite difference method for simulating large deformations of heterogeneous, viscoelastic materials. *Geophysical Journal International* 145 (1), 199–208.
- Schmidt, M.W., Poli, S., 1998. Experimentally based water budgets for dehydrating slabs and consequences for arc magma generation. *Earth and Planetary Science Letters* 163 (1–4), 361–379.
- Scholz, C.H., 1998. Earthquakes and friction laws. *Nature* 391 (6662), 37–42.
- Segall, P., Rice, J.R., 1995. Dilatancy, compaction, and slip instability of a fluid-infiltrated fault. *Journal of Geophysical Research - Solid Earth* 100 (B11), 22155–22171.
- Segall, P., Rice, J.R., 2006. Does shear heating of pore fluid contribute to earthquake nucleation? *Journal of Geophysical Research - Solid Earth* 111 (B9).
- Segall, P., Rubin, A.M., Bradley, A.M., Rice, J.R., 2010. Dilatant strengthening as a mechanism for slow slip events. *Journal of Geophysical Research - Solid Earth* 115 (B12).
- Shelly, D.R., Beroza, G.C., Ide, S., Nakamura, S., 2006. Low-frequency earthquakes in Shikoku, Japan, and their relationship to episodic tremor and slip. *Nature* 442 (7099), 188–191.
- Sibson, R., 1973. Interactions between temperature and pore-fluid pressure during earthquake faulting and a mechanism for partial or total stress relief. *Nature Physical Science* 243 (126), 66–68.
- Sibson, R.H., 1982. Fault zone models, heat flow, and the depth distribution of earthquakes in the continental crust of the United States. *Bulletin of the Seismological Society of America* 72 (1), 151–163.
- Sibson, R.H., 1990. Conditions for fault-valve behaviour. *Geological Society, London, Special Publications* 54 (1), 15–28.
- Sibson, R.H., 1998. Brittle failure mode plots for compressional and extensional tectonic regimes. *Journal of Structural Geology* 20 (5), 655–660.
- Skempton, A.W., 1960. Effective stress in soils, concrete, and rock. In: *Pore Pressure and Suction in Soils*. London, Butterworths pages 4–16.
- Song, T.-R.A., Helmberger, D.V., Brudzinski, M.R., Clayton, R.W., Davis, P., Pérez-Campos, X., Singh, S.K., 2009. Subducting slab ultra-slow velocity layer coincident with silent earthquakes in southern mexico. *Science* 324 (5926), 502–506.
- Sun, T., Ellis, S., Saffer, D., 2020. Coupled evolution of deformation, pore fluid pressure, and fluid flow in shallow subduction forearcs. *Journal of Geophysical Research - Solid Earth* 125 (3) e2019JB019101.
- Tentheorey, E., Cox, S.F., Todd, H.F., 2003. Evolution of strength recovery and permeability during fluid-rock reaction in experimental fault zones. *Earth and Planetary Science Letters* 206 (1–2), 161–172.
- Thielmann, M., Rozel, A., Kaus, B., Ricard, Y., 2015. Intermediate-depth earthquake generation and shear zone formation caused by grain size reduction and shear heating. *Geology* 43 (9), 791–794.
- Thomas, M.Y., Lapusta, N., Noda, H., Avouac, J.-P., 2014. Quasi-dynamic versus fully dynamic simulations of earthquakes and aseismic slip with and without enhanced coseismic weakening. *Journal of Geophysical Research - Solid Earth* 119 (3), 1986–2004.
- Tinti, E., Bazzarri, A., Piattesi, A., Cocco, M., 2004. Estimates of slip weakening distance for different dynamic rupture models. *Geophysical Research Letters* 31 (2).
- Tse, S.T., Rice, J.R., 1986. Crustal earthquake instability in relation to the depth variation of frictional slip properties. *Journal of Geophysical Research - Solid Earth* 91 (B9), 9452–9472.
- Vermeer, P., 1998. Non-associated plasticity for soils, concrete and rock. In: *Physics of Dry Granular Media*. Springer pages 163–196.
- Wada, I., Wang, K., He, J., Hyndman, R.D., 2008. Weakening of the subduction interface and its effects on surface heat flow, slab dehydration, and mantle wedge serpentinization. *Journal of Geophysical Research - Solid Earth* 113 (B4).
- Wang, K., 2007. Elastic and viscoelastic models of crustal deformation in subduction earthquake cycles. In: *The Seismogenic Zone of Subduction Thrust Faults* pages 540–575.
- Wang, K., Bilek, S.L., 2011. Do subducting seamounts generate or stop large earthquakes? *Geology* 39 (9), 819–822.
- Warren-Smith, E., Fry, B., Wallace, L., Chon, E., Henrys, S., Sheehan, A., Mochizuki, K., Schwartz, S., Webb, S., Lebedev, S., 2019. Episodic stress and fluid pressure cycling in subducting oceanic crust during slow slip. *Nature Geoscience* 12 (6), 475–481.
- Wassmann, S., Stoeckhert, B., 2013. Rheology of the plate interface–dissolution precipitation creep in high pressure metamorphic rocks. *Tectonophysics* 608, 1–29.
- Wu, Y., Chen, X., 2014. The scale-dependent slip pattern for a uniform fault model obeying the rate-and-state-dependent friction law. *Journal of Geophysical Research - Solid Earth* 119 (6), 4890–4906.
- Yarushina, V.M., Podladchikov, Y.Y., 2015. (De)compaction of porous viscoelastoplastic media: Model formulation. *Journal of Geophysical Research - Solid Earth* 120 (6), 4146–4170.
- Yi, J.T., Li, Y.P., Bai, S., Fu, Y., Lee, F.H., Zhang, X.Y., 2018. A simple effective stress approach for modeling rate-dependent strength of soft clay. *Journal of Offshore Mechanics and Arctic Engineering* 140 (4).